Experimental Characterization of Trapped Waves in a Mach 0.9 Jet By Rayleigh Scattering

Igor Kurek, Thomas Castelain, Pierre Lecomte, Emmanuel Jondeau, Christophe Bailly

forum acusticum 2023

EXPERIMENTAL CHARACTERIZATION OF TRAPPED WAVES IN A MACH 0.9 JET BY RAYLEIGH SCATTERING

Igor Kurek[1*] **Thomas Castelain**[1] **Pierre Lecomte**[1]
Emmanuel Jondeau[1] **Christophe Bailly**[1]
[1] Univ Lyon, Ecole Centrale de Lyon, CNRS, INSA Lyon,
Univ Claude Bernard Lyon I, LMFA, UMR5509, 69130, Ecully, France

ABSTRACT

Trapped waves in the potential core of high subsonic jet can be described as a system of waves responsible for a series of sharp peaks in the near-field pressure spectrum. In this work, density fluctuations associated with these acoustic waves in a Mach 0.9 jet are measured using Rayleigh scattering in the jet potential core. The set-up is installed in an anechoic wind tunnel, where simultaneous measurements of acoustic near-field pressure and flow density spectra are carried out. The lowest frequency and more prominent peak characteristic of trapped waves is observed at the same frequency in the acoustic and density spectra. The ability of the present setup to detect trapped waves signatures in the density spectrum is demonstrated.

Keywords: *Aeroacoustics, Jet noise, Rayleigh scattering, Optics, Experiments*

1. INTRODUCTION

The phenomenon of resonance recently identified [1] in the core of high subsonic jets, and referred to as trapped waves is easily observable in the acoustic field of the jet near the nozzle. The signature of these waves is a series of sharp peaks in the acoustic spectrum. Previous compressible large eddy simulation have made it possible to isolate these waves, and brought insights into their existence [1–3]. Experimental studies mainly focused on the characterization of this phenomenon from a purely acoustical viewpoint, by use of near-field measurements [4]. In the present work non-intrusive density measurements in a Mach 0.9 jet using a Rayleigh scattering technique along with acoustic measurements in the near field are performed. A continuous laser beam that illuminates the probed volume is used with a collecting optical setup to measure the intensity of Rayleigh scattered light from this volume. Density fluctuations measured outside the jet core were already studied for aeroacoustic purpose [5, 6], but its implementation in the jet core is proving challenging due to a low Signal-to-Noise Ratio (SNR) [7]. The present setup allows the detection of trapped waves signature in the density spectrum, due to a sufficiently high SNR. The paper is organized as follows: Section 2 exposes the principle of Rayleigh scattering measurements along with the experimental set-up used. The measurements are presented and analyzed in Section 3. Concluding remarks are finally given in Section 4.

2. DENSITY MEASUREMENTS FROM RAYLEIGH SCATTERED LIGHT

2.1 Measurement of Rayleigh scattered light

The phenomenon of scattering of light by particles smaller than the wavelength of the incident light is explained by the Rayleigh theory. The light is scattered in all directions, with intensity varying according to the angle Ψ between the polarization direction of the incident beam of wavelength λ and the direction of observation, as represented in Figure 1. There is no loss of energy during the scattering. The light power P_s scattered by the molecules present in a volume V_s is expressed as:

*__Corresponding author__: igor.kurek@ec-lyon.fr.

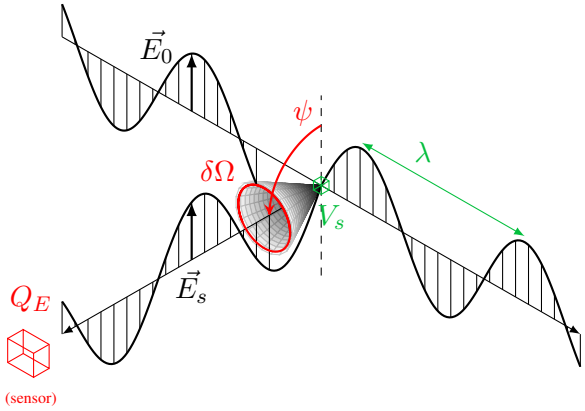

Figure 1. Diagram of the Rayleigh scattering intensity measurements. The incident and scattered light field are noted $\vec{E}_0$ and $\vec{E}_s$ respectively. The wavelength λ and the size of the probed volume V_s are dependent of the laser beam used. The polarization angle Ψ, the collecting angle $\delta\Omega$ and the efficiency Q_E of the sensor characterize the collecting optics.

$$P_s = \mathcal{N} V_s \frac{\partial \sigma^{\perp}}{\partial \Omega} \partial\Omega \sin^2(\psi) I_0 \tag{1}$$

where $\mathcal{N}$ is the numerical density. The term $\partial\sigma^{\perp}/\partial\Omega$ is the effective diffusion cross section of the molecule. It characterizes the ability of a molecule to scatter light. The solid angle over which the scattered light is collected is $\delta\Omega$. It depends on the collection optics used. The scattered power is of the order of 10^{-11} W for the device used, and thus cannot be measured by a power meter or photodiode. The power P_s is measured in the form of a photon flux of energy hc/λ, where h is Planck's constant and c is the speed of light in the medium. The measured photon flux is denoted Φ and is expressed as [8]:

$$\Phi = \underbrace{Q_E \delta\Omega V_s \frac{\lambda}{hc} \frac{N_a}{M} \frac{\partial \sigma^{\perp}}{\partial \Omega} \sin^2(\psi) I_0}_{=\kappa} \rho \tag{2}$$

with Q_E the quantum efficiency of the sensor represented by the red box in Figure 1, which defines the probability of a collected photon to be detected by it. The Avogadro number and the molar mass of air are N_A and M respectively. The term in underbrace in Eq. (2) is constant for a given experimental setup, and is denoted κ. It is determined in a calibration procedure, prior to each measurements [9].

2.2 Experimental setup

The measurement system is operated in an anechoic wind tunnel, and using an arrangement similar to [10]. The airstream is filtered an a low velocity co-flow is used to limit dust contamination of Rayleigh scattered light measurements [11]. The remaining dust signatures in the signal are removed in the post-processing, using an appropriate treatment [12]. The compressor feeds a convergent nozzle of 50 mm diameter D ((a) in Figure 2) at a Mach number M_j of 0.905±0.003. The Mach number is calculated from the static pressure and total temperature measured upstream of the nozzle, following the procedure described in [10]. In addition, an air dryer is mounted downstream of the compressor to limit the humidity of the jet, and the condensation of droplets due to the expansion at nozzle exit.
The acoustic measurement are performed using a 1/4" PCB® Piezotronics microphone located at $x/D = 0$ and $r/D = 1$, with x the axial coordinate of the jet and r the radial coordinate. The sampling frequency of the acoustic measurement is $f_{ac} = 204800$ Hz.

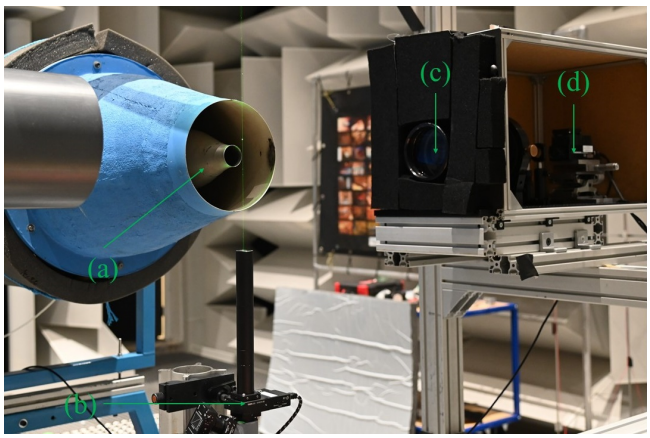

Figure 2. Photograph of the jet facility and optical setup. The laser beam is vertical and focused in front of the nozzle. The collecting optics are in the box at the top-right of the picture

The incident beam is emitted by a continuous fiber laser (ALS©-GR-65). The maximum power of the beam is 5 W, and the spectrum of the emitted light is centered on 532 nm. The orientation of the laser beam polarization

is controlled by a half-wave plate, placed in a motorized kinematic mount ((b) in Figure 2). The beam is then focused by a converging lens of focal length $f_l = 400\,\text{mm}$. The focal point of the laser beam defines the location of the measurement volume. The latter is placed for this study in the potential flow of a free jet. Finally, the laser beam is stopped by a beam dump. Light is collected by a set of two coupled converging lenses ((c) in Figure 2), with respective focal lengths $f_1 = 450\,\text{mm}$ and $f_2 = 200\,\text{mm}$ and of 110 mm diameter. A spatial filter, in the form of a rectangular pinhole of $200\,\mu m$ width, is placed at the focal point of the second lens. It is used to define the width of the measurement volume (here $600\,\mu m$). The light is then focused on the sensitive element of a Hamamatsu© H7422p-40 photomultiplier ((d) in Figure 2). The entire collection optics is placed in a black box, occluding light from the outside, except for a circular opening, in which the front lens of the collector is located. The output signal from the photomultiplier is digitized by a National Instrument™ NI-5160 digitizer. This system allows signal acquisition at a frequency of 1.25 GHz over a period of 0.86 s, which corresponds to 10^9 points. The signal is divided into time bins of duration dt, and the counting rate N correspond to the number of photons counted during each bin. This equivalent to sample N at a frequency $f_s = 1/dt$. The photon flux is therefore the numbers of photons counted N in a time bin, divided by its length dt, $\Phi(t) = N(t)/dt$.

2.3 Shot noise contribution

One of the major issue for time resolved measurements of the photon flux is the shot noise contribution [5]. As the arrival of photons on the sensor is random following a Poisson's law during an interval of time dt, the measurement obtained by photon counting is affected. It can be shown [12] that the signal to noise ratio (SNR) is given by:

$$\text{SNR} = \frac{\bar{N}}{\sigma_{\text{SN}}} = (\Phi dt)^{1/2} \tag{3}$$

where $\bar{N}$ is the expected number N of photons counted during a time interval dt and σ_{SN} is the shot noise standard deviation. The shot noise contribution can be neglected for mean density measurements where dt is high, but is superior to the density fluctuation ρ' contribution. However, it is statistically independent of ρ'. This property is used in the one-photomultiplier cross-spectrum method [12] to obtain density fluctuation spectra that are less altered by shot noise. The signal $N(t)$ with $t = 0,\ dt,\ 2dt, \ldots$ is divided in two sub-signals N_1 and N_2 respectively sampled from the original signal at $t = 2ndt$ and $t = 2ndt + 1$ with $n \in \mathbb{N}$. The signals are then divided into m segments N_1^j and N_2^j with $j = 1, 2, \ldots m$ that can overlap. The Fourier transform of each segment is denoted $F_{N_1^j}(f)$ and $F_{N_2^j}(f)$. The cross power spectral density (cpsd) between those two signals allows to greatly reduce its contribution, providing that m is large enough. It expresses as :

$$P_{N_1N_2}(f) = \frac{2}{m}\sum_{j=0}^{m-1} F_{N_1^j}(f)F^*_{N_2^j}(f) \tag{4}$$

where $*$ denotes the conjugate. The density fluctuation spectrum thus expresses as:

$$|P_{\rho'\rho'}(f)| \simeq \frac{f_s^2}{k}|P_{N_1N_2}(f)| \tag{5}$$

The larger m, the smaller the contribution of the shot noise to the mean cpsd. Therefore, the shot noise contribution can be reduced either by increasing the time interval dt and thus the SNR, or by considering a large number m of segments. It would respectively correspond to lower the sampling frequency f_s or to reduce the frequency resolution of the computed spectrum.

2.4 Calibration of the system

The calibration of the system is here based on the controlled modification of the polarization orientation determined by the angle Ψ in Eq. (2), of the beam illuminating the measurement volume [9]. The density remains constant, and is denoted ρ_0. By distinguishing this term in Eq. (2), a new constant κ' is introduced. Eq. (2) thus expresses as:

$$\Phi = \kappa' \sin^2(\Psi)\rho_0 + \Phi_{amb} \tag{6}$$

with Φ_{amb} the photon flux imputable to ambient luminosity. To perform this calibration, the polarization angle Ψ is driven by the changeable orientation of a half-wave plate placed on the optical path at the laser output and varies between 0 and π. The photon flux then varies over a range $\kappa'\rho_0$, and κ' is found by performing a non linear regression over the experimental data. The result of this procedure, realized in the potential core of a $M_j = 0.092$ jet, is shown in Figure 3, where $\kappa' = 3.27 \times 10^7$ photons.m^3.kg^{-1}.s^{-1}, and $\Phi_{amb} = 3.02 \times 10^6$

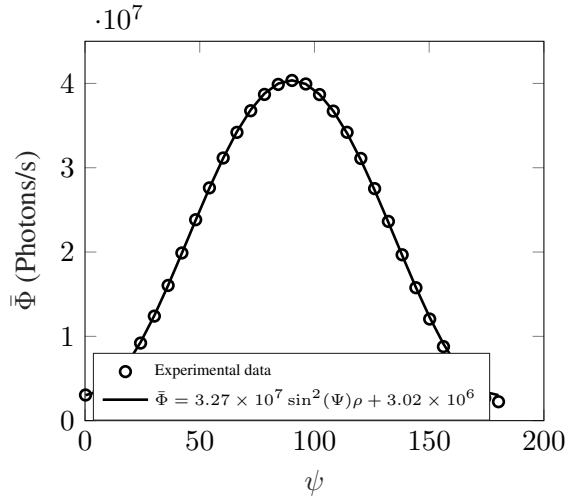

Figure 3. Calibration curve obtained by changing the polarization of the incident beam

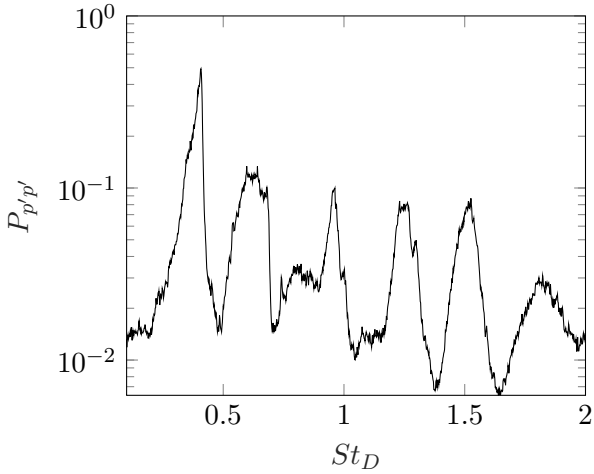

Figure 4. PSD of pressure fluctuations measured at $x/D = 0$ and $r/D = 1$. (near field microphone)

photons.s^{-1}. The following measurements are performed with $\Psi = 90°$ to maximize the photon flux.

3. RESULTS AND DISCUSSION

The power spectral density (PSD) of the pressure fluctuations measured with the microphone are shown in Figure 4. A series of peaks are observed, consistently with [2,4,7]. These are characteristic of the trapped waves. The more prominent peak is obtained for a nozzle diameter-based Strouhal number St_D of 0.4. Figure 5 shows PSD of density fluctuations in the jet core, at $x/D = 3$ and $r/D = 0$, normalized with ρ_j the mean density in the jet core and ρ_{amb} the ambient density. The PSD are the average PSD computed from the same 100 acquisitions, but with two sampling frequencies f_s. Based on Eq. (3) and the measured photon flux, reducing the sampling frequency from 102400Hz to 20000Hz leads to a SNR multiplied by 2. Both PSD are computed with the frequency resolution $\Delta f = 75$ Hz, corresponding to $m = 128$. The PSD computed from the signal sampled at the highest shows no peak. The spectrum is dominated by shot noise, and no clear feature is observable. A peak is clearly present at $St_D = 0.4$ on the red curve, which is the PSD of the signal sampled at 20000 Hz. This peak is at the same Strouhal number than the first peak found in the acoustic spectrum. It corresponds to the first axisymmetric radial mode, which is the more prominent for this jet. This peak was not observed in the experiments of [7], which was reported as the consequence of shot noise contamination of the signal.

A transversal profile of the magnitude of this peak is shown in Figure 6, along with the profile of the rms value of density fluctuations $\sigma_{\rho'}$ measured at $x/D = 1$, for $f_s = 20000$ Hz. At each position, 15 acquisitions are performed. The rms value of density fluctuations is determined using Parseval's identity:

$$\sigma^2_{\rho'} = \sum_{i=1}^{f_s/(2\Delta f)} |P_{\rho'\rho'}(i\Delta f)|\Delta f \qquad (7)$$

The peak magnitude forms a lobe in the center of the jet, which is again indicative of the first axisymmetric radial mode radial form [1]. It decreases when moving away from the center, and forms two sharp peaks in the turbulent shear layer, at $y/D \simeq 0.5$. The position of the shear layer is confirmed by of the profile of density fluctuations. A plateau in the potential core, and two peaks on the outer regions of the jet can be identified. This profile is similar to the results found by Rayleigh scattering measurements in [5].

4. CONCLUSION

Acoustic measurements were performed in the near field of a Mach 0.9 jet, along with density measurements inside the jet using Rayleigh scattering. The objective was to

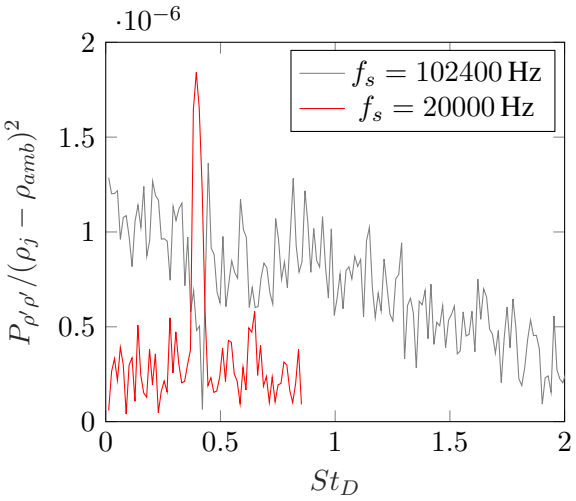

Figure 5. PSD of density fluctuations measured at $x/D = 3$ and $r/D = 0$. (Rayleigh scattering measurement)

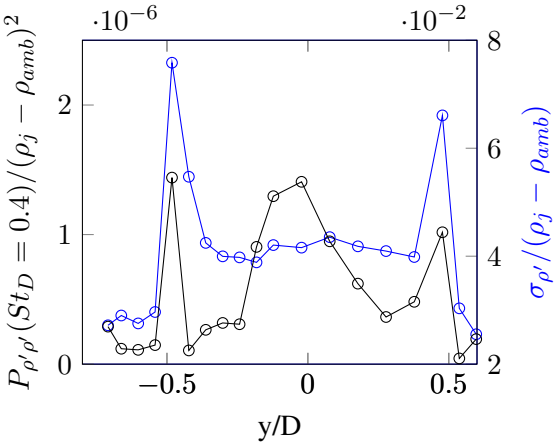

Figure 6. Transversal profile of $P_{\rho'\rho'}(St_D = 0.4)$ and rms fluctuations of density at $x/D = 1$

demonstrate the suitability of this non intrusive technique to measure density fluctuations in the jet core characteristics of the trapped waves.The experimental approach reveals a non-uniform distriution of the magnitude of the density fluctuations inside the jet core at a fixed axial distance from the nozzle. To capture this feature, SNR has been enhanced by adapting the treatment of the single-photomultiplier output.

5. ACKNOWLEDGMENTS

This work was performed within the framework of the industrial chair ARENA (ANR-18-CHIN-0004-01) co-financed by Safran Aircraft Engines and the French National Research Agency (ANR), and in the framework of the Labex CeLyA (ANR-10-LABX-0060) of the Université de Lyon, within the program "Investissements d'Avenir" (ANR-16-IDEX-0005) also operated by ANR.

6. REFERENCES

[1] A. Towne, A. V. G. Cavalieri, P. Jordan, T. Colonius, O. Schmidt, V. Jaunet, and G. A. Brès, "Acoustic resonance in the potential core of subsonic jets," Journal of Fluid Mechanics, vol. 825, pp. 1113–1152, Aug. 2017.

[2] C. Bogey, "Acoustic tones in the near-nozzle region of jets: Characteristics and variations between mach numbers 0.5 and 2," Journal of Fluid Mechanics, vol. 921, p. A3, Aug. 2021.

[3] C. Bogey, "Interactions between upstream-propagating guided jet waves and shear-layer instability waves near the nozzle of subsonic and nearly ideally expanded supersonic free jets with laminar boundary layers," Journal of Fluid Mechanics, vol. 949, p. A41, Oct. 2022.

[4] K. Zaman, A. Fagan, and P. Upadhyay, "Pressure fluctuations due to 'trapped waves' in the initial region of compressible jets," Journal of Fluid Mechanics, vol. 931, p. A30, Jan. 2022.

[5] J. Panda and R. G. Seasholtz, "Experimental investigation of density fluctuations in high-speed jets and correlation with generated noise," Journal of Fluid Mechanics, vol. 450, pp. 97–130, Jan. 2002.

[6] B. Mercier, T. Castelain, and C. Bailly, "Experimental investigation of the turbulent density – far-field sound correlations in compressible jets," International

Journal of Aeroacoustics, vol. 17, pp. 521–540, July 2018.

[7] A. F. Fagan and K. B. Zaman, "Rayleigh-scattering-based measurement of 'trapped waves' in high-speed jets," AIAA Aviation 2020 Forum, pp. 1–13, 2020.

[8] R. B. Miles, W. R. Lempert, and J. N. Forkey, "Laser rayleigh scattering," Measurement Science and Technology, vol. 12, no. 5, 2001.

[9] I. Kurek, T. Castelain, P. Lecomte, E. Jondeau, and C. Bailly, "Mesure de densité en écoulement par diffusion de rayleigh: Méthode de calibration par polarisation du faisceau incident," in 17ème Congrès Francophone de Techniques Laser (CFTL) 2022, Sept. 2022.

[10] B. André, Étude expérimentale de l'effet du vol sur le bruit de choc de jets supersoniques sous-détendus. PhD thesis, 2012.

[11] B. Mercier, Développement d'une méthode de mesure de la masse volumique par diffusion Rayleigh appliquée à l'étude du bruit de jet, et contribution à l'étude du screech dans les jets supersoniques sous détendus. PhD thesis, 2017.

[12] B. Mercier, T. Castelain, E. Jondeau, and C. Bailly, "Density fluctuations measurement by rayleigh scattering using a single photomultiplier," AIAA Journal, vol. 56, no. 4, pp. 1310–1316, 2018.